Model for surface packing and aeolian transport on sand ripples

M.Y. Louge*, A. Valance†, A. Ould el-Moctar**, D. Ould Ahmedou‡ and P. Dupont§

*Cornell University, Ithaca, NY (USA)
†Université de Rennes 1 (France)
**Ecole Polytechnique de Nantes (France)
‡Faculté des Sciences de Nouakchott (Mauritania)
§INSA de Rennes (France)

Abstract. Measurements indicate that the solid volume fraction on a sand ripple varies from random jammed packing at troughs to the minimum stable packing at crests. By relating variations of the solid volume fraction to those of the surface turbulent shear stress, a collisional model of reptation suggests a qualitative origin for these observations. Although the model overestimates the critical shear velocity at which reptation arises, it predicts the rate of aeolian transport on Earth and Mars.

Keywords: sand ripple, reptation, saltation, aeolian transport, Mars
PACS: 47.57.Gc, 42.68.Bz, 92.60.Gn

BACKGROUND

Desert winds mobilize sand by overcoming static friction and other surface forces. The resulting flow has particles "reptating" in a shear layer near the bed surface, and fewer, faster-moving "saltating" grains accelerated by the free stream before impacting the reptating layer and bed at a grazing angle [1]. Such bombardment dislodges particles from the bed, brings them into reptation, and gives them initial fluctuation kinetic energy.

We exploited the technique of Louge, et al [2] to record the solid volume fraction ν on a dry sand ripple of nearly monodisperse sand near Akjoujt (Mauritania). As Fig. 1 shows, ν varied from the random jammed packing $\nu_c \approx 0.64$ at troughs to the minimum value $\nu_m \approx 0.545$ for a stable packing at crests [3]. Here, we present a collisional model of reptation suggesting an origin for these variations and predicting the rate of aeolian transport.

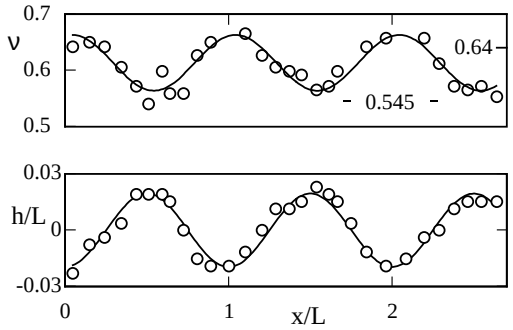

FIGURE 1. Surface profiles of solid volume fraction ν (top graph) and dimensionless ripple elevation h/L (bottom graph) along the direction x/L of prevailing winds blowing from left to right. Lines are best harmonic fits to the data with ripple amplitude $h_0 \simeq 2.8$ mm and wavelength $L \simeq 145$ mm. On the top graph, horizontal marks locate $\nu = \nu_c$ and $\nu = \nu_m$.

MODEL

The model treats reptation as a dense, steady shear layer of flowing grains driven by the surface turbulent shear stress τ_0. It is based on four relatively crude assumptions.

First, grains of diameter d and material density ρ_s are sufficiently agitated to interact through binary collisions. This allows us to adopt the constitutive relations of Jenkins and Richman [4], who calculate transport coefficients in terms of the "granular temperature" $T \equiv (1/3) < v_i' v_i' >$, where $v_i' \equiv \widetilde{v}_i - v_i$, $\widetilde{v}_i$ is the instantaneous grain velocity, and v_i is its average over time.

Second, we ignore any modification of τ_0 by suspended particles and write $\tau_0 = \rho u^{*2}$, where ρ is the gas density and u^* is the shear velocity. However, from Hunt, et al. [5], we recognize that the stress varies as

$$\tau_0 = \bar{\tau}_0[1 + (h_0/L) f(x/L)] \qquad (1)$$

along the wind direction x perpendicular to the ripple of amplitude h_0 and wavelength L. In Eq. (1), $\bar{\tau}_0$ is the average shear stress on a flat surface, and f is a periodic function of x/L that Gong, et al. [6] measured.

Third, ignoring infrequent bombardment of saltating grains, we assume that grain velocity fluctuations on top of the reptation layer are driven by gas turbulence. Thus, at the layer's free surface, denoted by the subscript 0, we

adopt the coupling of Pourahmadi and Humphrey [7]

$$3T_0 = 2k/(1+\mathrm{St}), \tag{2}$$

where $k \equiv < u_i' u_i' > = u^{*2}/C_\mu^{1/2}$, $C_\mu \simeq 0.09$ [8], and u_i' is the fluctuation gas velocity. The Stokes number $\mathrm{St} = \omega_s/\omega_L$ divides the particle relaxation time $\omega_s = \rho_s d^2/[18\mu(1+0.15\mathrm{Re}^{0.687})]$ by the Lagrangian turbulent integral time scale ω_L in the particle frame. Clift, et al. [9] corrected ω_s for high particle Reynolds number $\mathrm{Re} = \rho d\sqrt{2k}/\mu$ based on rms fluid velocity, where μ is the molecular viscosity of the gas. The integral time scale $\omega_L = (C_T/2)k/\varepsilon$ is roughly half its counterpart in the fluid frame [10], where $C_T \simeq 0.41$ [7]. The turbulent energy dissipation rate $\varepsilon = \varepsilon_g + \varepsilon_s$ in a unit fluid mass has a contribution $\varepsilon_g = C_\varepsilon \rho u^{*4}/\mu$ from the gas [8] and $\varepsilon_s = 2(\rho_s/\rho)[\nu_0/(1-\nu_0)](k/\omega_s)$ from solids [10], where ν_0 is the solid volume fraction on top of the reptation layer. We adopt $C_\varepsilon \simeq 0.25$ at the wall [8]. For typical conditions on Earth or Mars, $\mathrm{St} \gg 1$.

Fourth, because the reptation layer is dense, grains entrain air at their mean velocity. Thus, we ignore drag on reptating grains, making our analysis simpler than the more dilute sheet flow model of Jenkins and Hanes [11].

Reptation dynamics

Because ripples make an angle $< \arctan(2\pi h_0/L) \simeq 7^\circ$ to the horizontal, the component of gravity g along x is negligible. Instead, reptating grains are moved by τ_0. Because the reptation layer is thin, it is locally fully-developed and its force balance along x reduces to

$$\partial\tau/\partial y = 0, \tag{3}$$

and downward along y:

$$\partial\sigma_y/\partial y + \rho_s g \nu = 0. \tag{4}$$

The constitutive relation for shear stress is

$$\tau = f_1(\nu)\rho_s d T^{1/2} \partial v_x/\partial y, \tag{5}$$

and that for normal stress on surfaces normal to y is

$$\sigma_y = -f_4(\nu)\rho_s T. \tag{6}$$

The local fluctuation energy balance is

$$-\partial q/\partial y + \tau\partial v_x/\partial y - \gamma = 0, \tag{7}$$

with flux of fluctuation energy

$$q = -f_2(\nu)\rho_s d T^{1/2}\partial T/\partial y, \tag{8}$$

and volume rate of fluctuation energy dissipation

$$\gamma = f_3(\nu, e)\rho_s T^{3/2}/d. \tag{9}$$

Jenkins and Richman [4] provide f_1 through f_4 in terms of the pair distribution $g_{12}(\nu)$ at contact and the coefficient of normal restitution e, which measures energy lost in binary impacts. Jenkins and Zhang [12] conveniently introduce an effective $e \simeq e_n - (\pi/2)\mu_f$ combining the usual kinematic normal restitution e_n and the Coulomb friction coefficient μ_f to capture collisional energy loss in a generic shear flow. To represent sand grains, we adopt $e_n \simeq 0.92$ and $\mu_f \simeq 0.05$ reported by Lorenz, et al. [13] for glass beads and find $e \simeq 0.85$.

Equations (3), (4), (7) and (8) are non-linear ODEs in τ, σ_y, T and q. We deduce ν from Eq. (6) by inverting $f_4(\nu)$ using a look-up table. On the free surface of the reptation layer at $y = 0$, we prescribe the shear stress $\tau = \tau_0 < 0$ and invoke the boundary conditions of Jenkins and Hanes [14] relating the normal stress

$$\sigma_{y0} = -2\nu_0\rho_s T_0 \tag{10}$$

and the temperature T_0, which is coupled to the gas turbulent kinetic energy through Eq. (2) and, ultimately, to τ_0. Because $\mathrm{St} \gg 1$, $\rho_s T_0 \approx \tau_0\, C_T(1-\nu_0)/(3\nu_0 C_\mu^{1/2})$ when $\varepsilon_s \gg \varepsilon_g$. If instead gas turbulent dissipation dominates, $\varepsilon_s \ll \varepsilon_g$, and $T_0/gd \approx 12 C_T(1+0.15\mathrm{Re}^{0.687})/(C_\varepsilon C_\mu \mathrm{Ar})$, which varies weakly with τ_0, but strongly with particle size through Archimedes' number $\mathrm{Ar} \equiv \rho_s \rho g d^3/\mu^2$. At $y = 0$, Jenkins and Hanes [14] also showed that the volume fraction satisfies $\nu_0 g_{12} = 1/4$ or $\nu_0 \simeq 0.16$, and that the flux vanishes at a horizontal free surface, $q_0 = 0$.

Parameters of this problem are $\tau_0^* \equiv \tau_0/(\rho_s g d)$, Ar and e. We solve the ODEs downward using a fourth-order Runge-Kutta procedure until the granular temperature reaches $T = 0$, which fixes the reptation layer thickness $y = h_\ell$. Typical profiles are shown in Fig. 2 (left).

Agitated shear layers do not exist at arbitrarily small τ_0^*. Because reptation occurs on an erodible bed that only dissipates fluctuation kinetic energy [15], its agitation is sustained if and only if the volumetric production rate of fluctuation energy in the second term of Eq. (7) exceeds the volumetric dissipation rate γ. Thus, as τ_0^* decreases, the shear layer loses its agitation and eventually collapses at a minimum surface shear stress τ_{0crit}^* below which Eqs. (3)-(10) have no solutions. For $0.6 < e < 0.99$, we calculate that, locally, the minimum shear velocity necessary to create an agitated reptation layer obeys

$$\rho u_{crit}^{*2}/(\rho_s g d) \equiv \tau_{0crit}^* \simeq 0.09 + 0.135(1-e^2)^{0.4} \times \exp[-(\mathrm{Ar}/\mathrm{Ar}_0)^{1/2}], \tag{11}$$

where $\mathrm{Ar}_0 \simeq 6000$. As expected, Eq. (11) predicts that reptation requires faster winds on Mars than on Earth.

Because crests locally experience a higher surface shear stress for the same mean wind velocity, the threshold value of the *mean* shear velocity $\bar{u}^*$ at which crest grains are first mobilized is lower than what

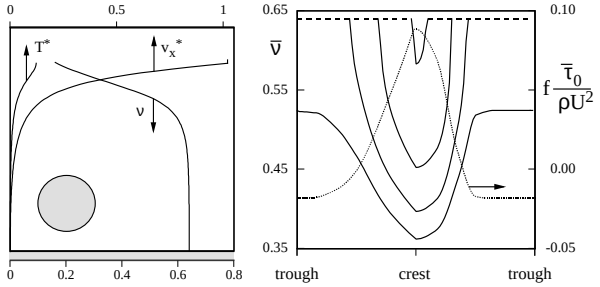

FIGURE 2. Model predictions for Ar $= 730$, $R_\rho = 2080$, $h_0/L = 0.02$ and $e = 0.85$, corresponding to 200μm grains of $\rho_s = 2500$kg/m^3 in air. Left: vertical profiles of solid volume fraction (bottom scale), dimensionless temperature $T^* \equiv T/gd$ and mean grain velocity $v_x^* \equiv v_x/\sqrt{gd}$ (top scale) in the reptation layer for $\tau_0^* = 0.153$. The darker region at the horizontal axis represents the top of the immobile sand bed. The circle shows grain size relative to the vertical axis. Gravity points downward. Right: predictions of $\bar{\nu}$ in the reptation layer from Eq. (14) (left axis) along the wind from trough to trough for $\mathrm{Fr}/\sqrt{\mathrm{R}_\rho} = 6.8, 8.5, 10.2$ and 12.1 (top to bottom solid lines). Where $\tau_0 < \tau_{0crit}$, reptation collapses and $\bar{\nu} = \nu_c$ (horizontal dashes). Dotted line, right axis: spline fit of $\bar{\tau}_0 f(x/L)/\rho U^2$ extrapolated from Gong, et al.'s data [6] using Eq. (1).

Eq. (11) predicts. For conditions of Fig. 2, we find $\bar{u}^* \approx 0.26\sqrt{\rho_s g d/\rho}$, which corresponds to a minimum wind speed $\simeq 13.6$ m/s to establish a reptation shear layer on the crest. (A velocity $\approx 65\%$ larger is necessary to mobilize the trough, which has a smaller surface shear stress).

This critical velocity is about twice that expected for the onset of ripples, which occurs at shear velocities just above the threshold [16, 17, 18]. By ignoring how this relatively dense particle suspension damps clear-gas turbulence at the surface, our analysis likely overestimates turbulent velocity fluctuations there. Unlike vertical gas-solid flows for which turbulence is affected by large relative velocities between gas and solids, and thus can be enhanced or reduced depending on grain size [19], horizontal [20] or isotropic [21] flows appear to decrease turbulence intensity at high loadings. In this context, because τ_{0crit}^* decreases with increasing C_μ or decreasing C_T, any reduction in k at the surface would lower our prediction of the critical surface shear stress.

Volume fraction evolution along a ripple

The mean volume fraction in the reptation layer is

$$\bar{\nu} = \frac{1}{h_\ell}\int_{y=0}^{h_\ell} \nu dy, \tag{12}$$

in which we exploit Eq. (4) to calculate the integral,

$$\bar{\nu} = -[\sigma_y(y = h_\ell) - \sigma_{y0}]/(\rho_s g h_\ell). \tag{13}$$

This prediction is conveniently represented by

$$\bar{\nu} = \nu_\infty + (\nu_c - \nu_\infty)\exp\{-[(\tau_0^* - \tau_{0crit}^*)/\tau_{0s}^*]^{1/2}\} \tag{14}$$

with $\nu_\infty \simeq 0.27$, $\tau_{0s}^* \simeq 0.17$, and τ_{0crit}^* from Eq. (11).

Using Eq. (1), the data of Gong, et al. [6] can be extrapolated to conditions other than their experiments using $\tau_0^* = (\mathrm{Fr}^2/R_\rho)(\bar{\tau}_0/\rho U^2)[1 + (h_0/L)f(x/L)]$, where $\bar{\tau}_0/\rho U^2 \approx 0.0015$ or, equivalently $u^*/U \approx 0.039$.[1] In this expression, $\mathrm{Fr} \equiv U/\sqrt{gd}$ is the Froude number based on wind velocity U, and $R_\rho \equiv \rho_s/\rho$. Accordingly, solid lines in Fig. 2 (right) shows how $\bar{\nu}$ evolves from a ripple trough to the next: $\bar{\nu}$ decreases with increasing dimensionless wind speeds; because troughs have the lowest τ_0^*, their reptation layer is denser.

Although this analysis explains why crests have smaller $\bar{\nu}$, it will remain qualitative until it captures the critical shear velocity more closely, perhaps by accounting for long-lasting contacts as reptation collapses [22], for the role of saltation splash in modifying T_0 and q_0, and for non-linear dynamics of ripple formation [23]. Meanwhile, we suggest that reptation gradually deposits loose granular material at crests from sand extracted from denser troughs. Thus, ripple crests grow in successive strata to produce a region of low ν consistent with observations in Fig. 1.

Aeolian transport

We calculate the mass flow rate $\dot{m}_{rept}$ of reptating grains in a unit direction parallel to the ripple crest line,

$$\dot{m}_{rept} = \int_0^{h_\ell} \rho_s \nu v_x dy, \tag{15}$$

by introducing $V \equiv v_x(h_\ell) - v_x$ subject to the ODEs $\partial V/\partial y = -\tau_0/(f_1\rho_s d T^{1/2})$ from Eq. (5) and $\partial J/\partial y = \rho_s \nu V$, which we solve with $V = 0$ and $J = 0$ at $y = 0$. Imposing $v_x = 0$ at $y = h_\ell$, we then deduce the velocity profile $v_x = V(h_\ell) - V$ and find $\dot{m}_{rept} = h_\ell \rho_s \bar{\nu} V(h_\ell) - J(h_\ell)$. We take $\dot{m}_{rept} = 0$ wherever $\tau_0 < \tau_{0crit}$.

As Jenkins and Hanes [14] implied, agitation at the free surface of a sheared granular layer launches ballistic grains aloft to a height $\sim T_0/g$. We assume that such grains are instantly accelerated to the speed $V_s = (u^*/\kappa)\ln(1 + T_0/gz_0)$ of the turbulent boundary layer [6] at that height. Here, $z_0 \approx d/30$ is a measure of aerodynamic roughness [1], $u^* = \sqrt{\tau_0/\rho}$ is the local shear velocity, which evolves along the ripple according to Eq. (1) and f in Fig. 2, and $\kappa \approx 0.4$ is von Karman's

[1] Figure (6b) of Gong, et al. [6] has a mislabeled vertical scale ten times greater than it should be.

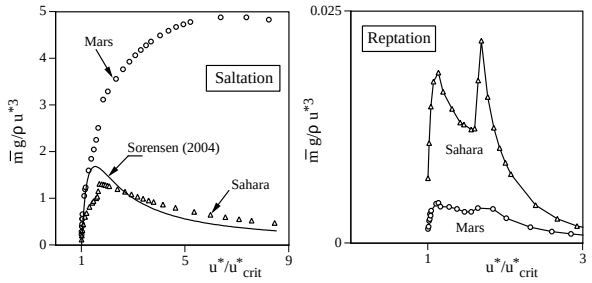

FIGURE 3. Dimensionless aeolian transport rate $\bar{m}\,g/(\rho u^{*3})$ averaged along a ripple vs. shear velocity relative to its threshold. Earth conditions are those of Fig. 2; on Mars, Ar = 10.5, $R_\rho = 10^5$. Left: triangles (Sahara) and circles (Mars) represent the saltation transport model of Eq. (17); the solid line is Sørensen's formula [24] in Eq. (18) with $\alpha_s = 0$ and the threshold shear stress $\tau^*_{0crit} \simeq 0.0123$ of Shao and Lu [17] for cohesionless grains. Right: reptation transport model of Eq. (15); up and down variations arise from averaging over the ripple, on which reptation collapses wherever $\tau_0 < \tau_{0crit}$.

constant. A vertical force balance reveals that ballistic grains have a mass per unit area

$$\int_{y=-\infty}^{0} \rho_s \nu dy = -\sigma_{y0}/g. \tag{16}$$

Then, using Eqs. (1) and (10), the local saltation mass flow rate per unit flow width is

$$\dot{m}_{salt} = \int_{-\infty}^{0} \rho_s \nu V_s dy = \tag{17}$$
$$2\rho_s \nu_0 \frac{T_0}{\kappa g}\sqrt{\frac{\bar{\tau}_0}{\rho}\left[1+\left(\frac{h_0}{L}\right)f\left(\frac{x}{L}\right)\right]}\ln\left[1+\frac{T_0}{gz_0}\right]$$

wherever $\tau_0 > \tau_{0crit}$, and zero otherwise. Figure 3 (left) shows the corresponding average saltation transport rate $\bar{m}_{salt}$ over the entire ripple. We compare it in dimensionless form to Sørensen's empirical formula [24]

$$\frac{\bar{m}_{salt}\,g}{\rho u^{*3}} = \left(1-\frac{1}{W^2}\right)\left[\alpha_s + \frac{\beta_s}{W^2} + \frac{\gamma_s}{W}\right], \tag{18}$$

where $W \equiv u^*/u^*_{crit}$, and $\beta_s \approx 0.41 + d/d_\beta$ and $\gamma_s \approx 0.8 + d/d_\gamma$ with $d_\beta \simeq 65\ \mu$m and $d_\gamma \simeq 140\ \mu$m.

Figure 3 confirms that sand transport is dominated by saltation [1]. It shows that our model agrees reasonably well with Sørensen's Eq. (18) and captures the peak in $\bar{m}\,g/(\rho u^{*3})$ that he reported. However, while his formula does not distinguish between martian and terrestrial conditions, our model predicts that, on Mars, $\bar{m}\,g/(\rho u^{*3})$ is greater at the same $\bar{u}^*/\bar{u}_{crit}$. This is because, in our model of gas-solid turbulence coupling at the surface, $T_0^* \propto \mathrm{Ar}^{-1}$, and Mars' Archimedes number is smaller than Earth's.

ACKNOWLEDGMENTS

This work was funded by the "Ministère de la Recherche" and "Agence Nationale de la Recherche" under grants ACI-500270 and ANR-05-BLAN-0273. MYL was supported by NSF travel grant INT-0233212.

REFERENCES

1. B. Andreotti, *J. Fluid Mech.* **510**, 47–70 (2004).
2. M. Y. Louge, R. Steiner, S. C. Keast, R. Decker, J. Dent, and M. Schneebeli, *Cold Regions Sci. & Technol.* **25**, 47–63 (1997).
3. M. Y. Louge, A. Valance, A. Ould el-Moctar, and P. Dupont, *J. Geophys. Res.* (2009), under review.
4. J. T. Jenkins, and M. W. Richman, *Arch. Rat. Mech. Anal.* **87**, 355–377 (1985).
5. J. C. R. Hunt, S. Leibovich, and K. J. Richards, *Quart. J. Roy. Met. Soc.* **114**, 1435–1470 (1988).
6. W. Gong, P. A. Taylor, and A. Dörnbrack, *J. Fluid Mech.* **312**, 1–31 (1996).
7. F. Pourahmadi, and J. Humphrey, *Phys.-Chem. Hydrodyn.* **4**, 191–219 (1983).
8. V. Patel, W. Rodi, and G. Scheuerer, *AIAA J.* **23**, 1308–1319 (1985).
9. R. Clift, J. Grace, and M. Weber *Bubbles, Drops and Particles*, Academic Press, New York, 1978.
10. J. D. Kulick, J. R. Fessler, and J. K. Eaton, *J. Fluid Mech.* **277**, 109–134 (1994).
11. J. T. Jenkins, and D. M. Hanes, *J. Fluid Mech.* **370**, 29–52 (1998).
12. J. T. Jenkins, and C. Zhang, *Phys. Fluids* **14**, 1228–1235 (2002).
13. A. Lorenz, C. Tuozzolo, and M. Louge, *Experimental Mechanics* **37**, 292–298 (1997).
14. J. T. Jenkins, and D. M. Hanes, *Phys. Fluids A* **5**, 781–783 (1993).
15. J. Jenkins, and E. Askari, *J. Fluid Mech.* **223**, 497–508 (1991).
16. J. D. Iversen and B. R. White, *Sedimentology* **29**, 111-119 (1982).
17. Y. Shao and H. Lu, *J. Geophys. Res.* **105**, 22437-22443 (2000).
18. B. Andreotti, P. Claudin, and O. Pouliquen, *Phys. Rev. Lett.* **96**, 028,001 (2006).
19. C. T. Crowe, *Int. J. of Multiphase Flow* **26**, 719–727 (2000).
20. J. Kussin, and M. Sommerfeld, *Experiments in Fluids* **33**, 143–159 (2002).
21. W. Hwang, and J. K. Eaton, *J. Fluid Mech.* **564**, 361–393 (2006).
22. R. Delannay, M. Louge, P. Richard, N. Taberlet, and A. Valance, *Nature Materials* **6**, 99–108 (2007).
23. A. Valance, *Eur. Phys. J. B* **45**, 433–442 (2005).
24. M. Sørensen, *Geomorphology* **59**, 53-62 (2004).